Available online at www.sciencedirect.com
SCIENCE DIRECT
Agricultural and Forest Meteorology 136 (2006) 132–146
AGRICULTURAL AND FOREST METEOROLOGY
www.elsevier.com/locate/agrformet

Upscaling fluxes from tower to landscape: Overlaying flux footprints on high-resolution (IKONOS) images of vegetation cover

J. Kim [a,b,*], Q. Guo [a], D.D. Baldocchi [a], M.Y. Leclerc [c], L. Xu [a], H.P. Schmid [d]

[a] *Ecosystem Science Division, Department of Environmental Science, Policy and Management, 151 Hilgard Hall, University of California, Berkeley, CA 94720, USA*
[b] *Department of Atmospheric Sciences and Global Environment Laboratory, 542 Science Hall, Yonsei University, Seoul 120-749, Republic of Korea*
[c] *Laboratory for Environmental Physics, University of Georgia, Griffin, GA 30223-1797, USA*
[d] *Department of Geography, Indiana University, Bloomington, IN 47405, USA*

Received 19 March 2004; received in revised form 6 September 2004; accepted 12 November 2004

Abstract

In this paper, we describe the process of assessing tower footprint climatology, spatial variability of site vegetation density based on satellite image analysis, and sensor location bias in scaling up to 1 km × 1 km patch. Three flat sites with different vegetation cover and surface heterogeneity were selected from AmeriFlux tower sites: the oak/grass site and the annual grassland site in a savannah ecosystem in northern California and a slash pine forest site in Florida, USA. The site vegetation density was expressed in terms of normalized difference vegetation index (NDVI) and crown closure (CC) by analyzing the high-resolution IKONOS satellite image. At each site, the spatial structure of vegetation density was characterized using semivariogram and window size analyses. Footprint maps were produced by a simple model based on the analytical solution of the Eulerian advection–diffusion equation. The resulting horizontal arrays of footprint functions were then superimposed with those of NDVI and CC. Annual sensor location biases for the oak/grass and the pine forest sites were <4% for both NDVI and CC, requiring no flux corrections in scaling from tower to landscape of 1 km^2. Although the annual grassland site displayed much larger location biases (28% for NDVI, 94% for CC), their temporal changes associated with averaging time showed a real potential to develop algorithms aimed at upscaling tower fluxes to the landscape in an effort to provide validation data for MODIS products.

Keywords: AmeriFlux; Footprint climatology; IKONOS; MODIS; NDVI; Upscaling

1. Introduction

Natural vegetation is spatially heterogeneous. In particular, the spatial variability of vegetation density influences the lower atmospheric circulation and surface exchange of energy, water and carbon over a wide range of scales (e.g., Shen and Leclerc, 1995; Buermann et al., 2001; Cosh and Brutsaert, 2003). The scaling process involves taking spatial, temporal and process information at one scale and using it to derive information at another scale (Jarvis, 1995). In this process, the extraction of ecophysiologically significant information depends on spatial and temporal scales at which data are collected (Rahman et al., 2003). For example, field researchers employing micrometeorological flux measurement techniques are constrained by the predetermined spatial (<10^4 to 10^6 m^2) and

* Corresponding author. Tel.: +1 82 2 2123 2691; fax: +1 82 2 312 5691.
E-mail address: joon-kim@yonsei.ac.kr (J. Kim).

0168-1923/$ – see front matter © 2005 Elsevier B.V. All rights reserved.
doi:10.1016/j.agrformet.2004.11.015

temporal (e.g., hours to years) resolution of the tower flux footprint (Baldocchi et al., 2001; Falge et al., 2002; Foken and Leclerc, 2004). On the other hand, multi-temporal, coarser remote sensing data allow mapping of the approximated surface flux over a wider region ($>10^6$ to 10^{12} m^2) and longer time period (from days to decades). At present, bridging the gap between these two scales is a major challenge facing the research community. Accurate assessments of regional- and global-scale changes in the biosphere depend on the definition of practical scaling logic relevant to current flux sites, logic which incorporates a combination of field measurements, remote sensing, and ecological modeling.

The footprint of turbulent flux measurements characterizes its spatial structure that varies with wind direction, surface roughness, measurement height, and atmospheric stability (e.g., Leclerc and Thurtell, 1990; Schmid, 2002). Recent development of footprint models provides diagnostic tools to quantify the representativeness of tower flux measurements for selected sites (e.g., Schuepp et al., 1990; Leclerc and Thurtell, 1990; Horst and Weil, 1994; Schmid, 1997; Baldocchi, 1997; Amiro, 1998; Schmid and Lloyd, 1999; Leclerc et al., 2003a,b; Soegaard et al., 2003; Foken and Leclerc, 2004; Levy et al., 2004). Despite many current studies on detailed footprint modeling and experimental validation (e.g., Leclerc and Thurtell, 1990; Wilson and Swaters, 1991; Horst and Weil, 1994; Finn et al., 1996; Leclerc et al., 1997, 2003a,b; Cooper et al., 2003), the temporal and spatial variability of footprints has not yet been investigated and the associated influence of varying site vegetation density on tower flux measurements. One of the practical problems in using a footprint model as an operational tool is that the source contribution in the area of a prospective measurement site is not known a priori. Recently, it has been demonstrated that long-term patterns of source contributions (i.e. 'footprint climatology') provide essential information about the vegetation sampled when measuring long-term fluxes especially over heterogeneous landscapes (e.g., Amiro, 1998; Schmid and Lloyd, 1999; Stoughton et al., 2000; Levy et al., 2004). The footprint climatology can be combined with information on the spatial variability of vegetation density characteristics provided by satellite image analysis. The current remote sensing technology provides high-resolution images of vegetation density in the form of the normalized difference vegetation index (NDVI) and crown closure (CC). The use of both the very high-resolution IKONOS imagery and the in situ flux footprint should result in more accurate validation data for process models and MODIS products.

Our objective is to examine the representativeness of tower fluxes in scaling up to the scale of satellite images (1 km × 1 km) by overlaying information of spatial variability of vegetation density on that of the flux footprint. The null hypothesis tested is that there is no significant difference in the flux indices used (NDVI, CC) between those averaged over the satellite domain and those selected and weighted by the footprint criteria. Accordingly, we selected three AmeriFlux sites with different vegetation densities to examine the influence of patch-scale heterogeneities on flux footprints of eddy-covariance towers. High-resolution IKONOS satellite images are used to determine NDVI and CC in the vicinity of the three sites. Footprint maps were produced using an analytical solution of the two-dimensional Eulerian advection–diffusion equation (Horst and Weil, 1994). The resulting horizontal arrays of footprint functions are then superimposed with those of NDVI and CC. The result is a 'tower location bias' (Schmid, 1997) which should be taken into account with the use of remote sensing and biosphere models to scale tower fluxes and field measurements. The present study also examines the spatial structure of vegetation density at the sites using semivariogram and window size analyses. Finally, 16 days averages of sensor location biases for NDVI and CC were estimated throughout the year and their temporal changes related to both the MODIS data product and the gross primary production from eddy-covariance flux measurements.

2. Methods and materials

2.1. Study sites

2.1.1. Savannah sites

Two sites (i.e., oak/grass and grassland) were selected in a savannah ecosystem in California, USA. The typical climate is characterized by dry summers and wet winters with average air temperature of 16.3 °C and precipitation of 559 mm.

The grassland flux tower is located in a grazed grassland clearing (38.413356°N, 120.950581°W, and 129 m above m.s.l.) in the same savannah, approximately 3 km southeast of the oak/grass flux tower. The soil is mostly rocky silt loam (*Lithic haploxerepts*). The vegetation is dominated by cool-season C_3 species such as *Brachypodium distachyon*, *Hypochaeris glabra*, and *Trifolium dubium*. The maximum canopy height is about 0.55 m during the peak growth stage in late spring (Xu and Baldocchi, 2003). The prevailing wind direction is mainly from southwest to northwest during

daytime and from northeast to southeast during nighttime.

The oak/grass flux tower is located on the foothills of Sierra Nevada (38.430994°N, 120.965831°W, and 177 m above m.s.l). The dominant tree species is blue oak (*Quercus douglasii*) with average canopy height of 7.1 m and maximum leaf area index of 0.6. The tree density is approximately 194 stems per hectare with mean diameter at breast height of 0.199 m and its basal area of 18 m^2 ha^{-1} (Xu et al., 2003). Throughout the year, the prevailing wind direction is from south to west during daytime and from northeast to southeast during nighttime.

2.1.2. Forest site

The third flux tower is located in an almost perfectly flat and homogeneous forest consisting primarily of managed slash pine (*Pinus elliottii* L.) on private land (29°44′N, 82°9′W) near the Austin-Cary Memorial Forest of the University of Florida, Gainesville, FL, USA. The tower is in a location of the forest where the trees are at mid-rotation (12 years old) in a sub-tropical climate. The forest has a closed canopy with an average height of 11.5 m in 2002. An area logged in the fall of 2000 formed an arc from the North to the West and Southwest 350–500 m away from the fIux tower. The soil type is sandy, siliceous and thermic (*ultic alaquods*) (Leclerc et al., 2003a). These three sites provide us with a unique opportunity to examine the influence of patch-scale heterogeneities outside the footprint (yet within the satellite domain) on flux footprints of eddy-covariance towers (Fig. 1).

2.2. Flux measurements

The fluxes of energy, water and CO_2 over the grassland and oak/grass sites have been measured continuously with eddy-covariance systems since October 2000 and March 2001, respectively. The flux systems were mounted at 2 m on the grassland tower and 23.4 m on the oak/grass tower and consisted of a tri-axial sonic anemometer (Model 1352, Gill Instruments Ltd., Lymington, England) and an open-path infrared gas analyzer (IRGA, Li 7500, Li-Cor Inc., Lincoln, NE, USA). The sampling rate was 10 Hz and the raw data from each 30 min period were stored on a laptop computer (Xu and Baldocchi, 2003, 2004). Measured fluxes were coordinate-rotated such that half-hourly mean vertical and lateral wind speeds were set to zero (Wesely, 1970).

Flux measurements at the forest site have been made intermittently since March 2000. Among other towers, the 28 m tower was instrumented with tri-axial sonic anemometers (Campbell Scientific, Logan, UT) along with fast response analyzers for tracer flux measurements. The sonic anemometer data were recorded at 8 Hz by a CR-10X logger (Campbell Scientific, Logan, UT). One of the towers at the forest site was also equipped with portable weather station sensors and provided half-hourly mean observations of air temperature, wind speed and direction, relative humidity, solar and net radiation, atmospheric pressure and rainfall (Leclerc et al., 2003a).

2.3. Footprint model

Eddy-covariance flux measurements are representative of the weighted average of the upwind surface flux and the term, *flux footprint*, describes this contribution of each element of the upwind surface to the measured flux. Here, we limit the footprint to areas upwind of the flux sensor and ignore the relatively small possibility of downwind contributions (Baldocchi, 1997). The vertical scalar flux measured at a point on the tower is thus

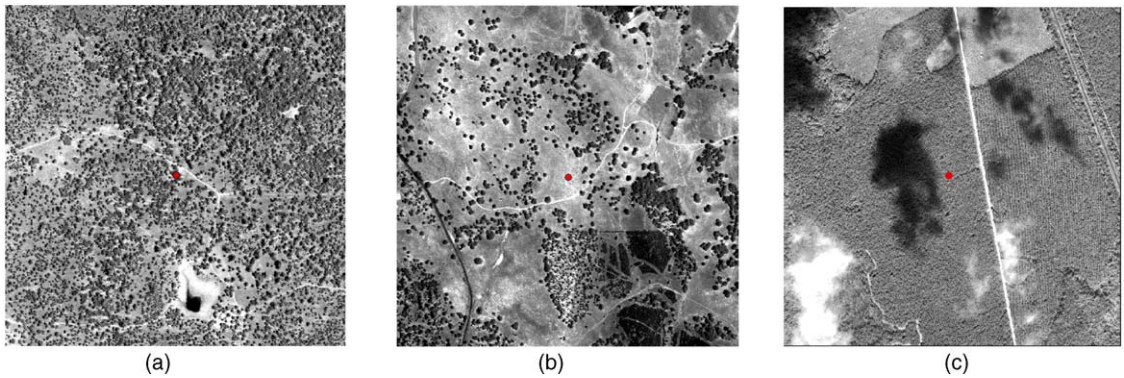

Fig. 1. Images of the three sites, showing a 1 km × 1 km square around the flux tower (located at the center of each image), from the IKONOS panchromatic band, with 1 m spatial resolution: (a) oak/grass savannah, (b) grassland opening in savannah, and (c) slash pine forest plantation.

the integrated contribution from all upwind source areas weighted by the footprint function and is defined as (e.g., Horst and Weil, 1992):

$$F(0,0,z_m) = \int_{-\infty}^{\infty}\int_{0}^{\infty} Q(x,y,z = z_0)\, f(x,y,z_m - z_0)\, dx\, dy, \quad (1)$$

where $F(0, 0, z_m)$ is the vertical eddy flux measured at the effective height, $z_m = z - d$, where z is the instrument height and d is zero-plane displacement; $Q(x, y, z_0)$ the source strength at upwind location (x, y) at the surface; z_0 the surface roughness length; $f(x, y, z_m - z_0)$ the flux footprint describing the flux portion seen at $(0, 0, z_m)$; and x, y, and z correspondingly represent streamwise, crosswind, and vertical distance from the tower base (0, 0, 0). It is assumed that the effective height of all sources and sinks is at the zero-plane displacement height.

Flux footprint functions can be computed by various approaches. The most common are: (1) analytical solutions to the advection–diffusion equation; (2) the Lagrangian stochastic simulation; and (3) large-eddy simulations (Foken and Leclerc, 2004 for a review). The latter two formulations are ideally suited to study the footprint behavior in complex flow conditions such as inside canopies and over complex heterogeneous surfaces. Since canopy geometry or sub-canopy diffusion is not considered in this study, an analytical footprint solution (FSAM, described in Schmid, 1997) based on Horst and Weil (1994) was selected to compute flux footprint on a half-hourly basis. The analytical solution relies on a sophisticated formulation of the two-dimensional advection–diffusion equation (Van Ulden, 1978) using parameters (Gryning et al., 1987) experimentally tested in Finn et al. (1996). This analytical solution takes into account both atmospheric stability and logarithmic wind profile above the canopy. The model input parameters are the effective height; the Obukhov length (L); the surface roughness length (z_0); the friction velocity (u_*); and the crosswind turbulence intensity σ_v/u_*, where σ_v is the standard deviation of lateral wind speed fluctuations. The model assumes a Gaussian distribution in the crosswind direction and is restricted to surface layer scaling conditions. The reader is referred to Horst and Weil (1994) and Schmid (1997) for more details.

As an independent check, flux footprints from the above analytical solution approach were compared against those from the Lagrangian stochastic simulation of Baldocchi (1997). In the latter, the vertical and horizontal dispersion was numerically simulated by calculating the Lagrangian trajectories of marked particles whose instantaneous velocities were reproduced based on the Langevin equation. The Lagrangian time scale was determined using the ratio of the Lagrangian length scale to the standard deviation of the vertical velocity and took into account atmospheric stability (Baldocchi, 1997). The required input parameters are z_m (measurement height), d (zero-plane displacement), z_0, L, u_*, σ_w (standard deviation of the vertical velocity), the particle release height and desired number of particles. The sonic anemometer data were directly used to calculate u_*, L, σ_v, and σ_w and indirectly used to deduce the information on d and z_0.

2.4. Estimation of zero-plane displacement

As a prerequisite to the footprint analysis, the zero plane displacement for each tower site was estimated using different methods depending on the data availability. At the savannah site, wind profile measurements were not available for either of the oak/grass and grassland towers. At the oak/grass site, the oak trees were sparsely distributed with maximum LAI of 0.5–0.7 with mean canopy height of 7.1 m. The "effective zero-plane displacement" was therefore evaluated from the single-level sonic anemometer measurements only. Two approaches considered in this analysis were those of Rotach (1994) and Martano (2000). The latter is based on the Monin–Obukhov similarity law for the wind speed profile and is written as

$$U(z) = (u_*/k)\{\ln[(z-d)/z_0] - \psi[(z-d)/L, z_0/L]\} \quad (2)$$

where $\psi[(z - d)/L, z_0/L] = \psi[(z - d)/L] - \psi[z_0/L]$ is the integrated stability correction function. Eq. (2) is ultimately reduced to a simpler least-squares procedure for one variable and is minimized with respect to d, giving a direct estimate of d and z_0. Rotach's (1994) approach, on the other hand, is simpler and based on heat fluxes and velocity variance measurements in near free-convection conditions. Similarity theory suggests that the following relationship holds under unstable conditions (Wyngaard et al., 1971):

$$\sigma_T/T_* = -C_1(-z/L)^{-1/3} \quad (3)$$

where σ_T and T_* are the standard deviation of air temperature and the scaling temperature, respectively, and the parameter C_1 was set at 1.1 (e.g., Katul et al.,

1995; Asanuma and Brutsaert, 1998; Choi et al., 2004). We then introduced $z - d$ instead of z in Eq. (3) and varied d to find the closest correspondence to Eq. (3). For each estimate of d, the root-mean-square (RMS) difference between predicted and observed values of σ_T/T_* for the ensemble of all available runs was calculated. The selected d had the lowest RMS. Furthermore, it was found to vary with wind direction and to have an average value of 4.75 m ($\sim 0.68 h_c$) for the prevailing wind direction (i.e., 180–270°). The z_0 was found to be 0.92 m and was also estimated from values of u_*, u, z/L, d and stability-corrected profile relations.

At the grassland site, based on the empirical relationship with canopy height (Rosenberg et al., 1983), d and z_0 were estimated to be 0.16 and 0.03 m with h_c of 0.22 m in July 2001 when the IKONOS image was taken. At the slash pine forest site, d was estimated from the vertical array of sonic anemometer measurements and was found to be 7.5 m. The z_0 was estimated to be 1.1 m (Leclerc et al., 2003a).

2.5. Analysis of high-resolution (IKONOS) images

Our strategy is to use high-resolution satellite data in conjunction with field computation of flux footprint to test the feasibility of combining these maps to quantify the location bias of flux towers. The IKONOS image is a new frontier of remote sensing, which has only recently become commercially available. Despite the fact that this is still an expensive option compared to other coarser images, IKONOS affords a fine-scale tool for mapping without reliance on dated imagery (Hansen et al., 2002). Table 1 summarizes the specifications of IKONOS images used in this study. Two IKONOS images were acquired, covering the three sites, and were used to compute Normalized Difference Vegetation Index (NDVI) and tree crown closure (CC), as described below.

2.5.1. Normalized difference vegetation index

The NDVI is an expression of contrasting reflectance between red and near-infrared regions of a surface spectrum and can be directly related to green vegetation cover or measure of canopy density. It is defined as (Schowengerdt, 1997):

$$\mathrm{NDVI} = \frac{R_{\mathrm{NIR}} - R_{\mathrm{RED}}}{R_{\mathrm{NIR}} + R_{\mathrm{RED}}} \quad (4)$$

where R_{NIR} is the reflectance within the near-infrared (NIR) and R_{RED} is the reflectance within the red band. NDVI generally correlates with green LAI and biomass (e.g., Sellers, 1985; Myneni et al., 1995). Typically, larger values of NDVI indicate greener surfaces whereas towns and lakes have small values. In our study, the IKONOS red and near-infrared bands were used to compute NDVI.

2.5.2. Crown closure

The CC is defined as the percentage of the ground covered by vertically projected crown in a stand. It is often used as a measure of stand density. In our study, IKONOS panchromatic band with 1 m resolution was used to detect the distribution of trees. Unsupervised classification methods with initial six classes showed a satisfactory classification result. The classes 1 and 2 were interpreted as trees and further merged together to produce the tree cover map. A 1 m × 1 m window was used to compute the crown closure.

2.5.3. Semivariogram analysis

For numerous sites in FLUXNET, we need a quantitative spatial analysis that can provide a consistent

Table 1
The specifications of IKONOS images used in this study

Specifications	Pan-chromatic	Multi-spectral
Scene dimensions		
Savannah, CA	5.412 km × 7.885 km	5.412 km × 7.885 km
Pine forest, FL	10.744 km × 10.736 km	10.744 km × 10.736 km
Spatial resolution	1 m	4 m
Radiometric resolution	11 bits	11 bits
Spectral resolution	450–900 nm	445–516 nm (blue), 506–595 nm (green), 632–698 nm (red), 757–853 nm (near-infrared)
IKONOS site (date)	Tower location	Surface characteristics
Northern California, USA (22 July 2001)	38.430994°N, 120.965831°W	Oak/grass, savannah
Northern California, USA (22 July 2001)	38.413356°N, 120.950581°W	Grassland, savannah
Gainesville, FL, USA (21 September 2002)	29.756593°N, 82.163172°W	Slash pine plantation

framework to evaluate both the variability and homogeneity of individual sites. For this purpose, we focus on the spatial variability of the vegetation cover at the atmospheric microscale (~1 km) and apply the semivariogram analysis. It relies on fewer assumptions in contrast with autocorrelation functions or Fourier transform methods. Furthermore, the semivariogram is not tied to the choice of initial parameters (St-Onge and Cavayas, 1997).

The spatial variance between NDVI (or CC) values of any two distinct pixels depends on their separation distance, Δr (i.e., "lag"). The semivariance, $\gamma(\Delta r)$, of NDVI (or CC) values between any two pixels at a lag of Δr is expressed as (e.g., Rahman et al., 2003):

$$\gamma(\Delta r) = \tfrac{1}{2}[\mathrm{NDVI}(r) - \mathrm{NDVI}(r + \Delta r)]^2. \quad (5)$$

There are $N(\Delta r)$ pairs of observations within the 1 km × 1 km patch separated by a lag Δr and thus their semivariance is given by

$$\hat{\gamma}(\Delta r) = \frac{1}{2N}\sum_{i=1}^{N}[z(r_i) - z(r_i + \Delta r)]^2. \quad (6)$$

In our study, $\hat{\gamma}(\Delta r)$ is computed as an average over all directions (called "omnidirectional" semivariogram), in which the lag measurement Δr is regarded as a scalar. Because of changes in prevailing wind directions included in the footprint computation, we also computed $\hat{\gamma}(\Delta r)$ along a specific direction (called "directional" semivariogram). Finally, to quantify the spatial pattern, $\hat{\gamma}(\Delta r)$ was plotted against lag and then a theoretical model was fit through the data points in a sample semivariogram.

2.5.4. Window size analysis

We evaluated the spatial representativeness of the flux tower at different scales by computing the mean NDVI and CC within a window of varying size (ranging from 10 m × 10 m to 1800 m × 1800 m), centered at the flux tower. (Note that the results of semivariography depend not on a specific location (of a flux tower) but on the vector Δr.) Together with the sample semivariogram, the window size analysis can provide complementary and comprehensive information to optimize flux sampling procedures and address scaling issues.

2.6. Overlaying footprint map with NDVI and CC

To examine whether there is a significant difference in vegetation density statistics between those averaged for the IKONOS patch (1 km × 1 km with flux tower at the center) and those defined (and weighted) by the tower footprint criteria, the resulting horizontal arrays of footprint functions were superimposed with those of NDVI and CC as follows: (1) we ran the footprint model, FSAM, with inputs (i.e., z_m, d, z_0, u_*, L, and σ_v) obtained from field measurements and produced two-dimensional arrays of the source weighting function; (2) using ArcGIS 8.2 (ESRI), the arrays of the weighting function were geo-referenced into the same projection systems of the NDVI and CC maps; and (3) weighted (and unweighted) average of NDVI and CC were computed by overlaying the footprint-weighted maps with NDVI and CC maps using the Visual Basic Application for ArcGIS. The footprint-weighted NDVI was computed using a discrete adaptation of (1):

$$\mathrm{NDVI_f} = \sum_{i=1}^{N}(f_i \times \mathrm{NDVI}_i) \quad (7)$$

where N represents the total number of pixels in the weight array, f_i the footprint weighting function derived from FSAM, and NDVI_i is the value derived from the IKONOS image. For the unweighted NDVI, the same weight was given to all pixels. Similarly, the unweighted and weighted CCs were computed for the three tower sites.

2.7. Sensor location bias

The spatial representativeness of the footprint is given by the sensor location bias, Δ (Schmid, 1997):

$$\Delta = (\mathrm{NDVI_f} - \overline{\mathrm{NDVI}})^2/\overline{\mathrm{NDVI}}^2 \quad (8)$$

where $\mathrm{NDVI_f}$ is the footprint-weighted NDVI and $\overline{\mathrm{NDVI}}$ is the unweighted average over the domain of 1 km^2 with the tower at the center. Using NDVI and CC as flux indices, the distribution of the root bias ($=\sqrt{\Delta}$) was calculated at each site under different stability conditions (unstable, mildly unstable, and near neutral) for each 45° wind direction sector.

3. Results and discussions

3.1. Spatial variability of vegetation density

Prior to examining the flux footprints measured from the tower, it is crucial to – "*know thy site*" – be fully aware of the spatial characteristics of the three selected sites. As seen in Fig. 1, the panchromatic IKONOS images of the three sites display distinct spatial structures ranging from sparse (and heterogeneous) to dense (and homogeneous) vegetation cover. Several

features of the IKONOS images are worth noting: (1) the oak-grass savannah site shows a gradual NE–SW gradient in tree density and its directional dependence; (2) the annual grassland site is a forest opening surrounded by thinly and irregularly clumped oak trees; and (3) the slash pine forest site has a closed homogeneous canopy with logged areas (cut in the fall 1999) in the North to the West 300–500 m away from the tower, providing us with an opportunity to examine the influence of atmospheric microscale heterogeneities on flux footprint (Leclerc et al., 2003a). Also noted at the forest site is the contamination in its IKONOS image by cumulus clouds and their shadows unavoidable at that site due to active evapotranspiration from the plantation with ample supply of heat and moisture into this region.

3.1.1. Semivariogram analysis

The shape of the semivariogram provides information about the spatial structure. In general, both NDVI (Fig. 2a) and CC (Fig. 2b and c) produced asymptotic semivariograms, characterized by a rise of gradually decreasing slope to form a straight horizontal line called the *sill*. This is due to the fact that increasing the lag distance between two pixels (4 m × 4 m for NDVI and 1 m × 1 m for CC) increases the chance of observing a great difference between their values. The lag distance at which the asymptote, or *sill*, is reached is called the *range*, beyond which no spatial covariance among samples exists. The *range* is a measure of the spatial scale of heterogeneity whereas the *sill* reflects absolute amount of heterogeneity (e.g., Cohen et al., 1990). The *nugget* is an estimate of the variance at a lag of zero and represents the microscale variability at distances shorter than the smallest distance among samples, together with sampling error (Levesque and King, 1999).

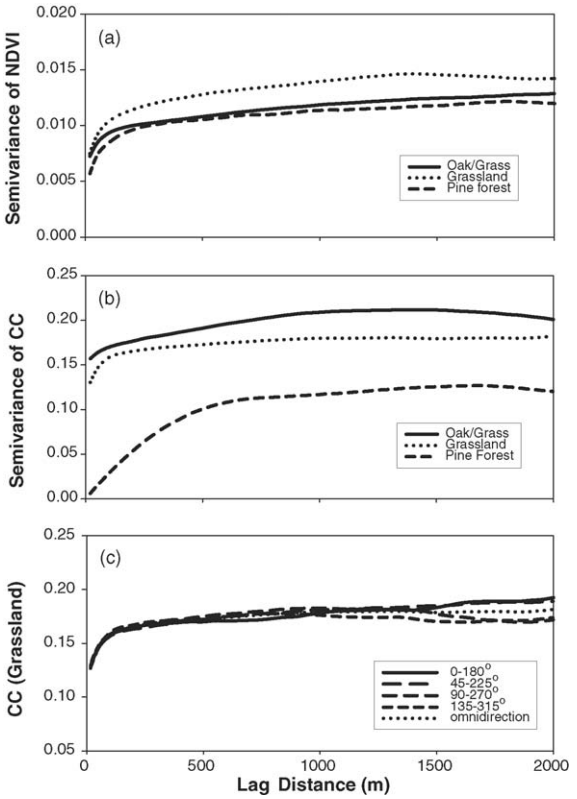

Fig. 2. Omnidirectional semivariograms for oak/grass savannah and grassland opening (in July 2001) and slash pine forest (in September 2002) for (a) NDVI, and (b) CC and (c) directional semivariograms of CC for grassland opening.

For NDVI at all three sites (Fig. 2a), the *range* is of the order of a few hundred meters suggesting that a tower with flux footprint confined within this *range* could potentially have a large bias in representing the landscape of 1 km^2. The annual grassland site demonstrates smaller range value (<200 m), indicating greater spatial dependency (i.e., heterogeneity). To our surprise, the clearcuts in the pine forest site do not significantly affect the *range* which remains relatively small. This is because replanted young pines have comparable NDVI to that of the pine forest. As expected with increasing total variance, the *sill* of the grassland is also larger due to greater variability in NDVI. There is no significant difference in *nugget* estimates between the oak/grass site and grassland site whereas the most homogeneous pine forest plantation displays the smallest *nugget*.

The semivariance of CC shows larger differences for each site (Fig. 2b). The oak/grass site displays a spherical semivariogram for a small lag of about 100 m and then shows a linear semivariogram up to a lag of 1000 m, indicating two main scales of heterogeneity (i.e., individual tree crown and forest canopy). The grassland opening and the pine forest sites, on the other hand, show distinctive spherical shape with the *range* of about 100 and 500 m, respectively. The large *range* value for the pine forest site is not necessarily an artifact mainly arising from the logged areas of zero crown closure. In comparison to the other two sites, the forest site displays a much smaller *sill* and the *nugget* of near zero because of the closed forest canopy.

The dependency of the semivariogram on the direction is known as the condition of anisotropy (e.g., Mohanty and Kanwar, 1997). The directional semivariogram can be obtained along transects but gives a better representation when computed in more than one direction. At the oak/grassland site, the directional semivariograms (at each 45°) of both NDVI and CC

show an increasing directional dependency (i.e., anisotropic) beyond a lag distance of about 200 m, corresponding to the value of the *range* (not shown). The directional semivariograms for the grassland site approach isotropy, showing a negligible dependence on the direction up to a lag distance of 1 km (Fig. 2c for CC only). The semivariograms of the pine forest site are also isotropic for NDVI but anisotropic for CC (not shown). Generally, sites with isotropic semivariogram are less vulnerable to directional location bias. However, in estimating the total amount of location bias, directional biases resulting from anisotropy may cancel out when the footprint climatology over a sufficient averaging domain is taken into consideration, as will be shown in the case of the oak/grassland site.

3.1.2. Window size analysis

The representativeness of a specific point (e.g., location of a flux tower) in the IKONOS images (Fig. 1) can be assessed with a window size analysis whereas no fixed points are considered in the above semivariogram analysis. The average NDVI and CC in windows of varying size are presented in Fig. 3. The NDVI at all three sites remains constant with the window width up to 2 km, except within the first 50 m or so where the data are contaminated with tower, small structures, buildings, and roads. The NDVI is highest at the forest site with an average of 0.52 while the coexisting two other sites in the same savannah eventually converge to 0.29 with increasing window width (Fig. 3a). The value of CC ranges from 0 (i.e., no trees—grassland opening) to 1.0 (i.e., full canopy—pine forest). The CC of the oak/grass site is steady at around 0.43 up to the window size of 1 km^2, beyond which it decreases with diminishing tree density as the grassland becomes more dominant. For the grassland site, CC is zero up to about 100 m and then immediately increases to 0.1 due to the presence of irregularly clumped oak trees surrounding this grassland opening. As the size of the window increases, the CC of the oak/grass and grassland sites gradually converges with one another. The pine forest site clearly displays the influence of clearcut areas on the estimate of CC as the window width becomes greater than 500 m.

Fig. 3 indicates that the tower flux measurement at the oak/grass site, for example, adequately represents NDVI and CC of the 1 km^2 as long as the footprint extends beyond the first 50 m or so. For the grassland opening site, a significant underestimation of both NDVI and CC is obvious unless the tower footprint stretches out several hundred meters. The result of this window size analysis suggests that this technique can be effectively used, in conjunction with a semivariogram,

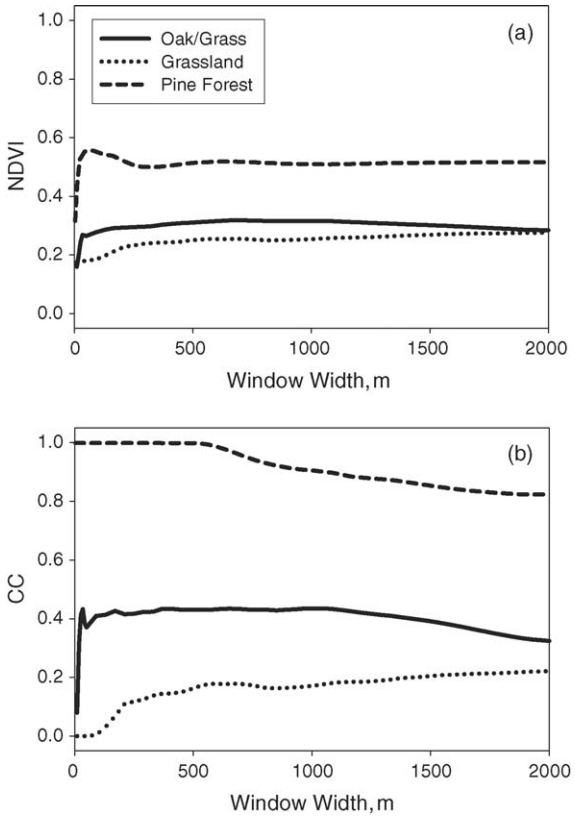

Fig. 3. The window-averaged NDVI and CC of varying size (with the flux tower located at the center of the window) for (a) NDVI and (b) CC.

to either evaluate the representativeness of the pre-existing flux tower or to perform an a priori optimization of flux sampling procedures in addressing scaling issues. In fact, directional analysis of window size for different wind sectors provides important new insight on sensor location bias associated with the footprint climatology of the tower flux. An exhaustive directional analysis can be made but the analysis can be better optimized when combined with the wind climatology around the flux tower.

3.2. Location bias distribution

To analyze the footprint-based distribution of location bias, we followed the methodology of Schmid and Lloyd (1999).

3.2.1. Flux footprint

Using the model FSAM of Schmid (1997), flux footprints from the analytical solution to the diffusion equation were calculated for the oak/grass site with z_m/z_0 of 20.3 in Fig. 4. Footprint computations were made for a prevailing wind direction of 225° for near-neutral

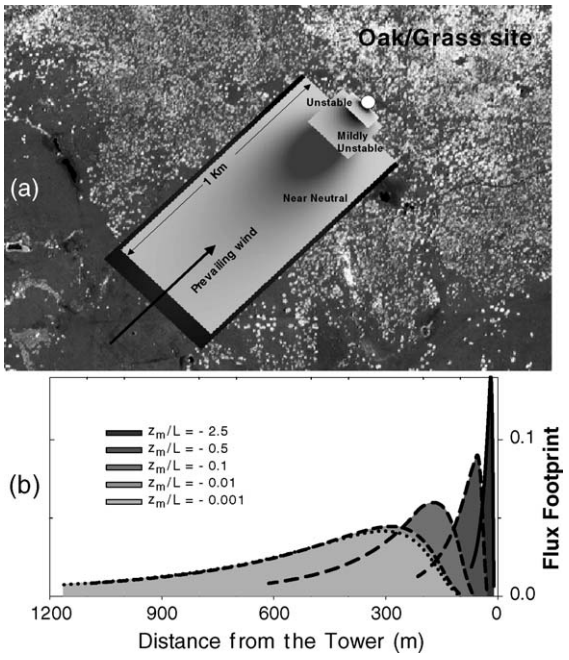

Fig. 4. Flux footprints (a) overlaid with IKONOS image and (b) upwind variation in the crosswind-integrated flux footprints at the oak/grass site under different stability conditions.

to stable conditions ($0.001 \geq z_m/L \geq -0.001$), mildly unstable conditions ($-0.1 < z_m/L < -0.001$), and unstable to strongly unstable conditions ($z_m/L \leq -0.1$). The scaled footprint values were produced at discrete intervals in two-dimensional arrays matching the spatial resolution of the NDVI and CC database. The resulting discretized footprint functions are then superimposed over the IKONOS image of the oak/grass site. The individual rectangle indicates what the eddy-covariance sensors mounted at $z_m/z_0 = 20.3$ on the tower sees of the flux from the oak/grass surface for different stability conditions. The darker shades indicate a greater source weight (Fig. 4a). Clearly, locations closer to the flux tower are more likely represented by the eddy-covariance measurement than locations further from the tower. Fig. 4b represents the crosswind-integrated flux footprint showing changes in peak amplitude and position under different atmospheric stability conditions. Under strongly unstable conditions, the size of the source area and of the footprint is markedly reduced to tens of meters. Under mildly unstable to near-neutral conditions, the greater footprint contains source area that stretches out to >1 km. Flux footprints under typical unstable conditions during daytime would lie between the above two extremes. The flux footprints for the other two sites are not shown here but their size increases and moves farther upwind of the tower with sensor height and the atmospheric stability encountered at each site.

3.2.2. Sensor location bias

The sensor location bias, Δ (i.e., the spatial representativeness of the footprint contents) was then computed for the three sites using Eq. (8). Fig. 5 shows the distribution of the root bias, $\sqrt{\Delta}$, over eight sectors of wind direction (45° each) in three stability categories around the periods when the IKONOS images were taken, using NDVI and CC as flux indices. Prior to the evaluation of footprint climatology, an examination of the absolute values of directional $\sqrt{\Delta}$ given in Fig. 5 provides useful insight. It is worth remembering that $\sqrt{\Delta}$, by definition, does not indicate the direction of the bias (e.g., positive/negative bias corresponds to over/underestimation). Overall, the homogeneous pine forest shows least $\sqrt{\Delta}$ of 5–10% for NDVI (and CC) and no directional dependency except during near neutral conditions for the sectors from 270° to 360° where the clearcuts are located (resulting in location bias of 15–30%). The grassland site, on the other hand, displays the largest $\sqrt{\Delta}$ (15–50% for NDVI and 60–100% for CC). The location bias at the oak/grass site is 5–20% for NDVI and 0–45% for CC with greater biases under unstable conditions. Here, large biases are not necessarily significant, if their occurrence is rare and/or associated with time when turbulent exchange is weak (e.g. nighttime stable conditions).

To examine this concept, measured wind directions and atmospheric stabilities over the two entire years were used to derive a footprint climatology.

3.2.3. Climatology of input parameters

Fig. 6 shows a composite 2-year wind rose based on the scaled climatology of input variables for the footprint model (mean horizontal wind speed, atmospheric stability, crosswind turbulence intensity) for the oak/grass and the grassland savannah sites. (The pine forest site was not included in this analysis due to discontinuous flux measurements for the 2 years considered here. Besides, the location bias was very small for all wind directions at this homogeneous site.) The wind direction and speed are wider and higher at the oak/grass site whereas the grassland site shows narrow range of prevailing wind directions with lower wind speeds. At both sites, there is a clear distinction in wind direction and the related stability condition between daytime (unstable with wind from 200° to 300°) and

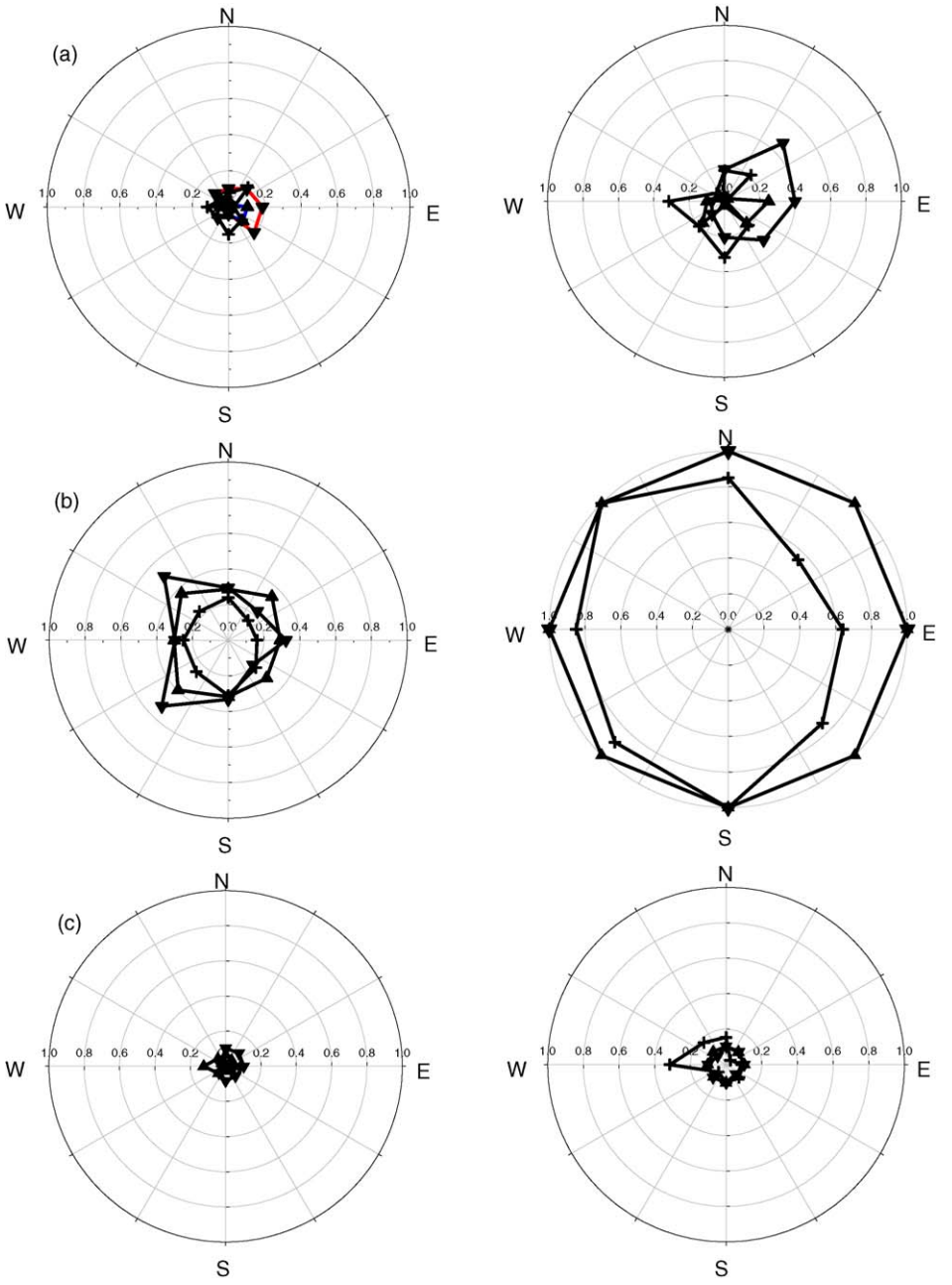

Fig. 5. Distribution of the root bias ($\sqrt{\Delta}$) over wind direction around the periods when IKONOS images were taken, using NDVI (left) and CC (right) as flux indices for (a) the oak/grass site, (b) the annual grassland site, and (c) the slash pine forest site in three stability categories (+, near neutral; ▲, mildly unstable; ▼, unstable conditions).

nighttime (stable with wind from 30° to 120°), suggesting the probable existence of significant directional biases for the site with anisotropy. The crosswind turbulence intensity needed to determine the lateral breadth of the footprint ranged from 2 to 4 at the oak/grassland site, with higher values for the grassland site.

3.2.4. Annual location bias

Fig. 7 shows root bias fractions for 16 wind direction sectors on a composite 2-year wind rose based on the scaled climatology of atmospheric stability for the footprint model at the oak/grass and the annual grassland sites. Here, we assume that the directional

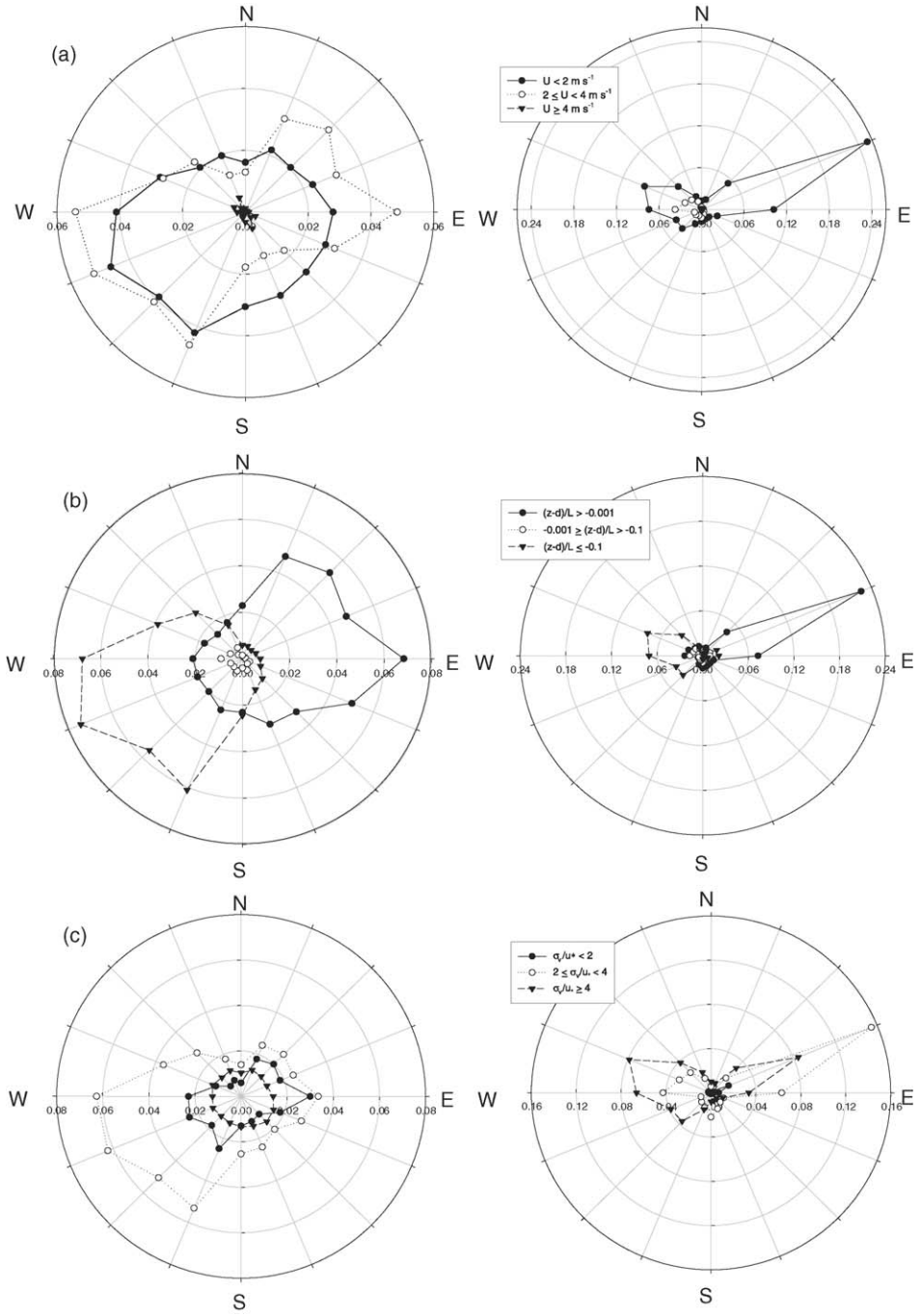

Fig. 6. Climatology of wind direction with (a) mean horizontal wind speed, (b) atmospheric stability and (c) crosswind turbulence intensity for the oak/grass site (left) and the grassland site (right) for 2 years (2001–2002).

root bias obtained from one IKONOS image (taken on 22 July 2001) would hold throughout the entire year of 2001 and 2002. This is a plausible assumption for CC, which would not change on a short-term basis (e.g., a few years) without natural (e.g., fire) or anthropogenic alterations (e.g., logged areas in the slash pine forest site). NDVI, on the other hand, changes seasonally. However, our analysis is sensitive to the relative variability of this index across the domain, not its absolute values. Thus, our use of just one IKONOS derived NDVI distribution to estimate footprint representativeness over an extended period relies on

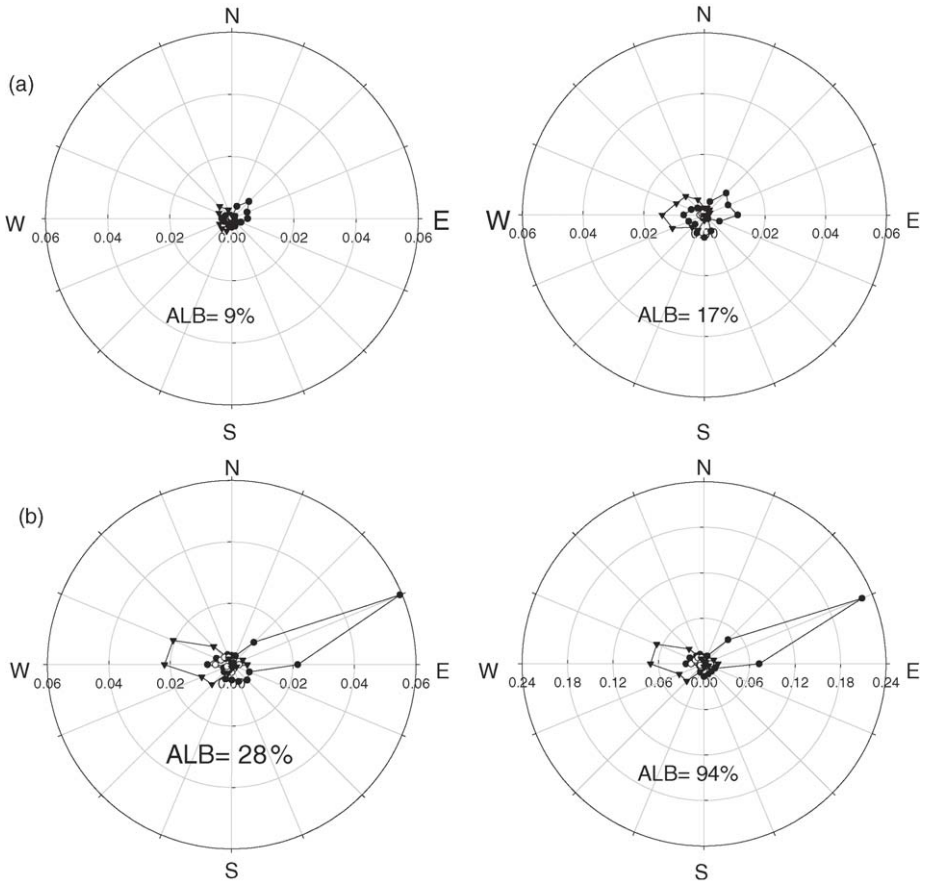

Fig. 7. Distribution of the annual root bias fractions over wind direction, using NDVI (left) and CC (right) as flux indices for (a) the oak/grass site and (b) the annual grassland site in three stability categories (●, near neutral to stable; ○, mildly unstable; ▼, unstable conditions). ALB is the annual location bias ($=\sum_{yr}(\sqrt{\Delta}) \times 100\%$).

the assumption that seasonal variations of NDVI affect all areas within our domain proportionally, with a similar phenological development.

The sum of these root bias fractions (for all three stability categories and wind directions) yields the annual location bias (ALB) (Fig. 7). For the two-year period studied, the annual location bias amounts to 9% and 17% of the cumulative NDVI and CC, respectively, at the oak/grass site. As expected, the annual grassland site shows a significant amount of ALB (28% for NDVI and 94% for CC). It should be noted that the absolute values of ALB could be misleading because individual root bias, $\sqrt{\Delta}$ by definition (Eq. (8)), no longer contains information on the sign of the bias. To examine this notion, the actual bias ($\delta = (\mathrm{NDVI_f} - \overline{\mathrm{NDVI}})/\overline{\mathrm{NDVI}}$ where the sign was preserved) was calculated for each wind direction (and stability conditions) and then multiplied by its relative frequency for the 2-year period. The resulting bias fractions are presented for the two savanna sites in Fig. 8. At the oak/grass site, bias fractions are distributed on both sides, resulting in smaller ALB of <4% for NDVI and ~0% for CC. At the annual grassland site, all the bias fractions are negative throughout the season, thereby underestimating NDVI and CC by 28% and 94%, respectively.

3.2.5. Temporal changes in location bias, NDVI/MODIS and GPP

Seasonal changes in the direction and magnitude of the estimated location biases for NDVI and CC over the course of the year (2001) are examined in Fig. 9. Also presented are the estimates of 16-day composites of 1 km^2 NDVI values (with the flux tower at the center) from the MODIS sensor (http://www.fluxnet.ornl.gov/fluxnet/modis2.cfm) and the relative gross primary production ($\mathrm{GPP_{REL}}$) from the eddy-covariance tower flux data (Xu and Baldocchi, 2003). To match with the MODIS–NDVI data, all other data are also presented as the averages for the 16-day interval. Again, the seasonal pattern of location bias for NDVI is partially

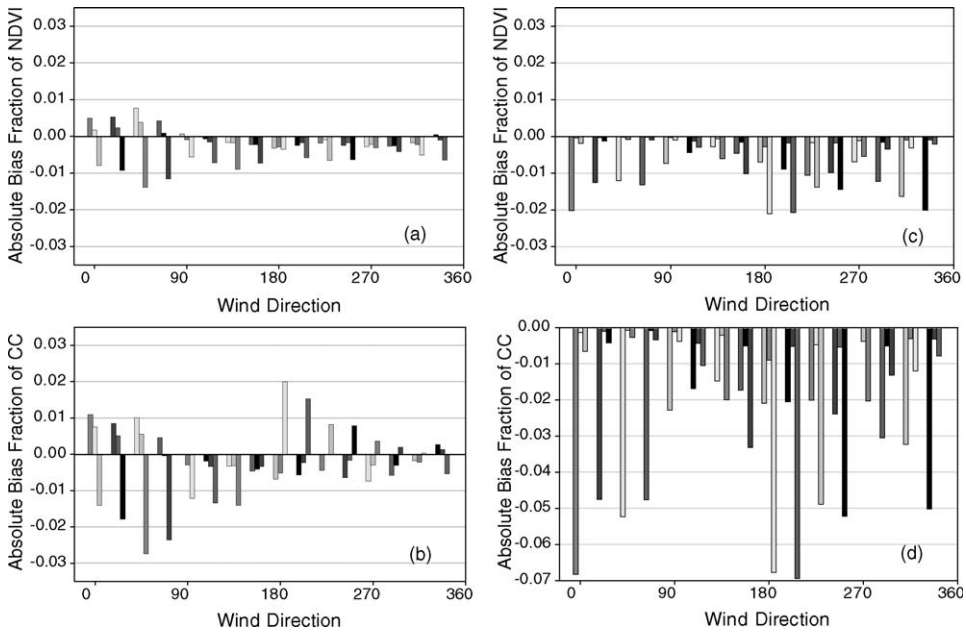

Fig. 8. The bias fractions, δ, for NDVI (top) and CC (bottom) based on actual bias multiplied by its relative frequency for the year 2001–2002 at the oak/grass site (left) and the annual grassland site (right).

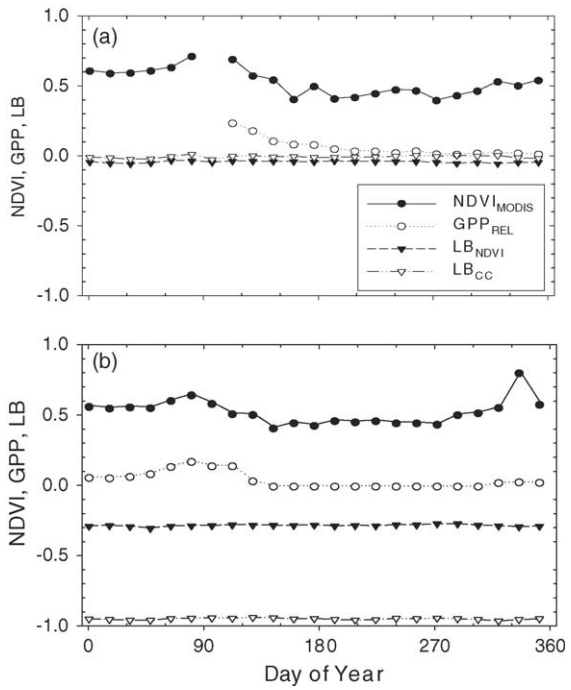

Fig. 9. Sixteen-day averages of NDVI from the MODIS sensor, relative gross primary production (GPP_{REL}, normalized by the annual sum) from tower flux measurements, and location biases for NDVI and CC for (a) the oak/grass site and (b) the annual grassland site in 2001.

limited by our use of a single IKONOS image for the whole year. However, it is clear in Fig. 9 that 16-day averages of location biases for both NDVI and CC are the same as their annual estimates. Furthermore, they do not show any variation throughout the year. It is obvious that the footprint climatology with a 16-day averaging time results in a similar effect to that produced with an annual averaging. When the half-hourly and daily averaging periods are used for footprint climatology, the standard deviations are, respectively, ±50% and ±10% of the annual location bias. When the averaging periods are 8–16 days, the standard deviation becomes virtually zero. It is also noted that there is a good agreement in seasonal patterns between the MODIS–NDVI and the relative GPP, suggesting that the information on location bias for NDVI can be effectively used for upscaling tower CO_2 fluxes to landscapes.

4. Summary and conclusions

In this paper, we have evaluated the relevance of estimates of tower CO_2 flux measurements in terms of spatial and temporal variability in source/sink strength distribution for three AmeriFlux sites. The temporal variability was accounted for by incorporating the effect of changing wind direction on tower flux footprints and by incorporating the diurnal cycles of stability-

dependent shrinking and expanding footprint domains into the vegetation density distribution, which was in turn related to the interpretation of net carbon exchange data.

As flux indices, we have used two parameters of vegetation density: normalized difference vegetation index and crown closure. The latter is more variable in space and less variable in time whereas the former is variable in both space and time depending on site heterogeneity and environmental conditions (e.g., drought). We accounted for spatial variability by integrating time-varying flux footprint maps to vegetation density maps (of NDVI and CC) obtained from high-resolution IKONOS image analysis. The resulting footprint-weighted NDVI and CC were then compared against the ''true'' average over the satellite domain of 1 km^2 with the flux tower at the center.

Our results show the location biases for NDVI and CC to be less than 5% at the oak/grass and the slash pine forest sites. For the annual grassland site, δ is 28% for NDVI and 94% for CC. Considering the inherent uncertainties in tower flux measurements, the satellite image analysis with the limited dataset selected (one image for the whole year), and the approximation of footprint climatology, a δ of 10% should be an acceptable criterion for testing our null hypothesis. We therefore conclude that there is no significant difference in flux indices (i.e., NDVI, CC) between those averaged for the satellite domain and those selected and weighted by the footprint criteria in the oak/grass site and the slash pine forest site. For the annual grassland site, however, scaling tower flux to a 1 km^2 patch would require caution and must take the large δ into account. Temporal variability of the resulting location bias over the year was examined along with 16-day averages of MODIS-based NDVI and tower flux-based GPP. The results suggested that the validation data for carbon flux products derived from satellites and/or models with grid size of $\sim$1 km^2 should be averaged at least for 4–8 days to properly incorporate the time and space scales involved in the measured processes.

The semivariogram and window size analyses are solely based on remote sensing data, which can be useful to provide important information in selecting tower location, or to pre-analyze the spatial heterogeneousness without detailed knowledge on meteorological data on the scene. A priori information on the degree of anisotropy is useful in flux footprint analysis in relation to the sensor location bias because of its strong dependence on site climatology of prevailing wind direction.

Acknowledgements

This study was funded by the US Department of Energy's Terrestrial Carbon Program, Grant No. 0006149 (Award register # ER63024 0006149). Joon Kim is also supported partly by the Ministry of Environment of Korea through ''The Eco-Technopia 21 Project'' and by the Climate Environment System Research Center of the Korean Science and Engineering Foundation. Our thanks go out to Drs. Steve Running and Sinkyu Kang for providing MODIS data.

References

Amiro, B.D., 1998. Footprint climatologies for evapotranspiration in a boreal catchment. Agric. For. Meteorol. 90, 195–201.

Asanuma, J., Brutsaert, W., 1998. Turbulence variance characteristics of temperature and humidity in the unstable atmospheric surface layer above a variable pine forest. Water Resour. Res. 35, 515–521.

Baldocchi, D., 1997. Flux footprints within and over forest canopies. Bound.-Layer Meteorol. 85, 273–292.

Baldocchi, D., Falge, E., Wilson, K., 2001. A spectral analysis of biosphere–atmosphere trace gas flux densities and meteorological variables across hour to multi-year time scales. Agric. For. Meteorol. 107, 1–27.

Buermann, W., Dong, J., Zeng, X., Myneni, R.B., Dickinson, R.E., 2001. Evaluation of the utility of satellite-based vegetation leaf area index data for climate simulations. J. Clim. 14, 3536–3550.

Choi, T., Hong, J., Kim, J., Lee, H., Asanuma, J., Ishikawa, H., Gao, Z., Ma, Y., Ueno, K., Wang, J., Koike, T., Yasunari, T., 2004. Turbulent exchange of heat, water vapor and momentum over a Tibetan prairie by eddy covariance and flux-variance measurements. J. Geophys. Res.

Cohen, W.B., Spies, T.A., Bradshaw, G.A., 1990. Semivariograms of digital imagery for analysis of conifer canopy structure. Remote Sens. Environ. 34, 167–178.

Cooper, D., Eichinger, W.E., Archuleta, J., Hipps, L., Kao, J., Leclerc, M.Y., Neale, C.M., Prueger, J., 2003. Spatial source-area analysis of three-dimensional moisture fields from lidar, eddy-covariance and footprint model. Agric. For. Meteorol. 114, 213–234.

Cosh, M.H., Brutsaert, W., 2003. Microscale structural aspects of vegetation density variability. J. Hydrol. 276, 128–136.

Falge, E.J., Tenhunen, D., Baldocchi, D.D., 2002. Phase and amplitude of ecosystem carbon release and uptake potentials as derived from FLUXNET measurements. Agric. For. Meteorol. 113, 75–95.

Finn, D., Lamb, B., Leclerc, M.Y., Horst, T.W., 1996. Experimental evaluation of analytical and Lagrangian surface-layer flux footprint models. Bound.-Layer Meteorol. 80, 283–308.

Foken, Leclerc, 2004. Methods and limitations in validation of footprint models. Agric. For. Meteorol. 127 (3–4), 223–234. (Special Issue: Footprints of Fluxes and Concentrations).

Gryning, S.E., Holtslag, A.A.M., Irvin, J.S., Sivertsen, D., 1987. Applied dispersion modeling based on meteorological scaling parameters. Atmos. Environ. 21, 79–89.

Hansen, M.C., DeFries, R.S., Townshend, J.R.G., Marufu, L., Sohlberg, R., 2002. Development of a MODIS tree cover validation data set for Western Province, Zambia. Remote Sens. Environ. 83, 320–335.

Horst, T.W., Weil, J.C., 1992. Footprint estimation for scalar flux measurements in the atmospheric surface layer. Bound.-Layer Meteorol. 59, 279–318.

Horst, T.W., Weil, J.C., 1994. How far is far enough? The fetch requirements for micrometeorological measurements of surface fluxes. J. Atmos. Oceanic Technol. 11, 1018–1025.

Jarvis, P.G., 1995. Scaling processes and problems. Plant Cell Environ. 18, 1079–1089.

Katul, G.G., Goltz, S.M., Hsieh, C.I., Cheng, Y., Mowry, F., Sigmon, J., 1995. Estimation of surface heat and momentum fluxes using the flux-variance method above uniform and non-uniform terrain. Bound.-Layer Meteorol. 74, 237–260.

Leclerc, M.Y., Shen, S., Lamb, B., 1997. Observations and large-eddy simulation modeling of footprints in the lower convective boundary layer. J. Geophys. Res. D 120, 9323–9334.

Leclerc, M.Y., Karipot, A., Prabha, T., Allwine, G., Lamb, B., Gholz, H.L., 2003a. Impact of non-local advection on flux footprints over a tall forest canopy: a tracer flux experiment. Agric. For. Meteorol. 115, 19–30.

Leclerc, M.Y., Meskhidz, N., Finn, D., 2003b. Comparison between measured tracer fluxes and footprint model predictions over a homogeneous canopy of intermediate roughness. Agric. For. Meteorol. 117, 145–158.

Leclerc, M.Y., Thurtell, G.W., 1990. Footprint predictions of scalar fluxes using a Markovian analysis. Bound.-Layer Meteorol. 52, 247–258.

Levesque, J., King, D.J., 1999. Airborne digital camera image semivariance for evaluation of forest structural damage at an acid mine site. Remote Sens. Environ. 68, 112–124.

Levy, P.E., Baldocchi, D.D., Grelle, A., Miller, S., Milne, R., Wofsy, S.C., 2004. Effects of spatial heterogeneity on sampling errors in CO_2 flux measurements over uneven-aged forests. Agric. For. Meteorol., submitted for publication.

Martano, P., 2000. Estimation of surface roughness and displacement height from a single-level sonic anemometer data. J. Appl. Meteorol. 39, 708–715.

Mohanty, B.P., Kanwar, R.S., 1997. A relative-flux-correction scheme for analyzing three dimensional data of a tile-drained agricultural plot. J. Hydrol. 194, 107–125.

Myneni, R.B., Los, S.O., Asrar, G., 1995. Potential gross primary productivity of terrestrial vegetation from 1982 to 1990. Geophys. Res. Lett. 22, 2617–2620.

Rahman, A.F., Gamon, J.A., Sims, D.A., Schmidts, M., 2003. Optimum size for hyperspectral studies of ecosystem function in southern California chaparral and grassland. Remote Sens. Environ. 84, 192–207.

Rosenberg, N.J., Blad, B., Verma, S.B., 1983. Microclimate: The Biological Environment. John and Wiley.

Rotach, M.W., 1994. Determination of the zero plane displacement in an urban environment. Bound.-Layer Meteorol. 67, 187–193.

Schmid, H.P., 1997. Experimental design for flux measurements: matching scales of observations and fluxes. Agric. For. Meteorol. 87, 179–200.

Schmid, H.P., 2002. Footprint modeling for vegetation atmosphere exchange studies: a review and perspective. Agric. For. Meteorol. 113, 159–183.

Schmid, H.P., Lloyd, C.R., 1999. Spatial representativeness and the location bias of flux footprint over inhomogeneous areas. Agric. For. Meteorol. 93, 195–209.

Schowengerdt, R.A., 1997. Remote Sensing: Models and Methods for Image Processing. Academic Press, San Diego, CA.

Schuepp, P.H., Leclerc, M.Y., McPherson, J.I., Desjardin, R.L., 1990. Footprint prediction of scalar fluxes from analytical solutions of the diffusion equation. Bound.-Layer Meteorol. 50, 355–374.

Sellers, P.J., 1985. Canopy reflectance, photosynthesis and transpiration. Int. J. Remote Sens. 6, 1335–1372.

Shen, S., Leclerc, M.Y., 1995. How large must surface layer inhomogeneities be before they influence the convective boundary layer structure? A case study. Quart. J. Roy. Meteorol. Soc. 121, 1209–1228.

Soegaard, H., Jensen, N.O., Boegh, E., Hasager, C.B., Schelde, K., Thomsen, A., 2003. Carbon dioxide exchange over agricultural landscape using eddy correlation and footprint modeling. Agric. For. Meteorol. 114, 153–173.

St-Onge, B.A., Cavayas, F., 1997. Automated forest structure mapping from high resolution imagery based on directional semivariogram estimates. Remote Sens. Environ. 61, 82–95.

Stoughton, T.E., Miller, D.R., Yang, X., Hendrey, G.M., 2000. Footprint climatology estimation of potential control ring contamination at the Duke Forest FACTS-1 experiment site. Agric. For. Meteorol. 100, 73–82.

Van Ulden, A.P., 1978. Simple estimates of vertical diffusion from sources near the ground. Atmos. Environ. 12, 2125–2129.

Wesely, M.L., 1970. Eddy correlation measurements in the atmospheric surface layer over agricultural crops. PhD Dissertation. University of Wisconsin, Madison, WI, USA.

Wilson, J.D., Swaters, G.E., 1991. The source area influencing a measurement in the planetary boundary layer: the footprint and the distribution of contact distance. Bound.-Layer Meteorol. 55, 25–46.

Wyngaard, J.C., Cote, O.R., Izumi, Y., 1971. Local free convection, similarity, and budgets of shear stress and heat flux. J. Atmos. Sci. 28, 1171–1182.

Xu, L., Baldocchi, D.D., 2003. Seasonal trend of photosynthetic parameters and stomatal conductance of blue oak (*Quercus douglasii*) under prolonged summer drought and high temperature. Tree Physiol. 23, 865–877.

Xu, L., Baldocchi, D.D., 2004. Seasonal variation in carbon dioxide exchange over a Mediterranean annual grassland in California. Agric. For. Meteorol. 123, 79–96.